Calculation of strain effects on vacancy-mediated diffusion of impurities in fcc structures: General approach and application to Ni_1 − −xSi_x

Thomas Garnier, Zebo Li, Maylise Nastar, Pascal Bellon, Dallas R. Trinkle

Calculation of strain effects on vacancy-mediated diffusion of impurities in fcc structures: General approach and application to Ni_{1−x}Si_{x}

Thomas Garnier, Zebo Li, Maylise Nastar, Pascal Bellon, and Dallas R. Trinkle

Phys. Rev. B **90**, 184301 — Published 3 November 2014

DOI: 10.1103/PhysRevB.90.184301

Calculation of strain effects on vacancy-mediated diffusion of impurities in fcc structures: a general approach and application to Ni(Si)

Thomas Garnier,[1,*] Zebo Li,[1] Maylise Nastar,[2] Pascal Bellon,[1] and Dallas R. Trinkle[1]

[1] *Department of Materials Science and Engineering, University of Illinois, Urbana-Champaign*

[2] *CEA, DEN, Service de Recherches de Métallurgie Physique, F-91191 Gif-sur-Yvette, France*

(Dated: September 16, 2014)

Abstract

Transport coefficients, the elements of the so-called Onsager matrix, are required for accurate mesoscopic simulations of kinetics or to predict macroscopic diffusion kinetic behavior. These coefficients can be significantly affected by strain. At the atomic scale, the effect of strain on atomic jump frequencies can be computed using density functional theory calculations. The present work shows how these results can be used to compute the strain-dependent Onsager matrix. Using an analytical method—the self-consistent mean field method—we compute analytical expressions of the Onsager matrix describing vacancy-mediated diffusion of impurities in face centered cubic structures under elementary strains. Also, we compute the derivatives of the Onsager matrix with respect to strain—the elasto-diffusion tensor—to investigate strain sensitivity of transport. We show that the atomic scale symmetry breaking induced by strain changes diffusion behavior qualitatively. This phenomenon is shown for the Ni(Si) alloy under tetragonal strain. The terms of the Onsager matrix are found to be non-Arrhenian, as well as their derivative with respect to strain. In this case, nonlinear effects leading to a solute drag reduction are identified.

The properties of structural and functional materials are often optimized by controlling their microstructure. The required microstructure usually corresponds to an out-of-equilibrium state of the alloy which is obtained during heat treatment. The evolution of this microstructure is often controlled by atomic diffusion, which affects the chemical homogenization of castings[1,2] or the rate of precipitation of second phases during heat treatments[3,4]. A stable microstructure is also required for the material to maintain its properties during use. Diffusion is an activated process which is usually very slow at room temperature. However, many applications subject the material to high temperature or irradiation thus enhancing diffusion[5]. One effect of irradiation in crystalline alloys is the creation of Frenkel pairs of point defects in the bulk. This supersaturation of point defects accelerates diffusion, and their elimination at sinks such as dislocations or free surfaces induces sustained atomic fluxes. Solute atoms can be dragged towards the vacancy sinks or away from them, depending on the kinetic correlations between solute and vacancy, leading to radiation-induced segregation and precipitation[6–9].

Defects such as dislocations or interfaces act as sinks for point defects but also generate a strain field, which alters diffusion properties[10–13]. By breaking the symmetry of the crystal structure, the strain field induces anisotropy of the diffusion properties[10,11,13] The Onsager matrix—which relates chemical potential gradients to atomic fluxes—is then a second-rank tensor. The Onsager matrix of diverse cubic structures has been computed[14–22]. However, anisotropic structures have received little attention, even if the impurity and matrix diffusion coefficients have been computed in some cases[23–26].

In a previous work, we investigated the effects of the stress field of an edge dislocation on Si impurities fluxes in Ni[27] using density functional theory (DFT) calculations to compute the diffusion properties at the atomic scale, and using this data to build the Onsager matrix. Ref. 28 details how the effect of strain on migration barriers for atomic jumps leading to diffusion can be calculated with DFT for this alloy. Here we demonstrate how these results can be used to compute the full Onsager matrix of an anisotropic system to produce the strain-dependent mesoscopic diffusion properties. First, the methods used are briefly reviewed. Next, some qualitative effects of strain on the Onsager matrix are then demonstrated using an ideal solid solution. Finally, the calculations of the Onsager matrix are applied to the case of the Ni(Si) alloy. For that system, the elasto-diffusion tensor that describes the effect of strain on the diffusion properties is provided, and symmetry breaking

and non-linear effects of strain on the Onsager matrix are discussed.

I. METHOD

At the atomic scale, diffusion is controlled by the frequency at which the exchanges between atoms and vacancies take place. This frequency depends on the local chemical environment. Using the notation introduced in Ref. 18, these frequencies can be written in the case of an infinitely dilute alloy A(B) as $w_{abc}^{(\zeta)}$, where a designates the vacancy-jumping atom vector symmetry class, b the solute-jumping atom symmetry class and c the vacancy-solute symmetry class, while $\zeta = 0$ for jumps in pure A, $\zeta = 1$ for jumps from a site in interaction with a solute toward another one, $\zeta = 2$ for a vacancy-solute exchange, $\zeta = 3$ for a jump dissociating the solute-vacancy pair and $\zeta = 4$ for an association jump. Moreover, within Vineyard's harmonic transition state equation[29], these frequencies are Arrhenius,

$$w_{abc}^{(\zeta)} = \nu_{abc}^{(\zeta)} e^{-E_{abc}^{\mathrm{mig},(\zeta)}/(k_{\mathrm{B}}T)}, \tag{1}$$

where k_{B} is the Boltzmann constant, T is the temperature, $\nu_{abc}^{(\zeta)}$ is the attempt frequency, and $E_{abc}^{mig,(\zeta)}$ is the migration enthalpy. In the following, we omit unnecessary indices in ν and E^{mig} when no confusion is possible (e.g., $w_a^{(2)}$). Both ν and E^{mig} are sensitive to the chemical environment and to the strain field, and can be computed with DFT[28].

At the mesoscopic scale, in a near equilibrium system, the atomic flux per unit area J_α of a chemical species α (including vacancies V) is related to the gradients of chemical potential $\nabla(\mu_\beta/k_{\mathrm{B}}T)$ of all atomic species β by the Onsager matrix $L_{\alpha\beta}$[30],

$$J_\alpha = -\sum_\beta L_{\alpha\beta} \nabla \left(\frac{\mu_\beta}{k_{\mathrm{B}}T} \right). \tag{2}$$

Hence, the Onsager matrix generalizes the diffusion coefficients to the case of non-ideal mixtures. It also quantifies kinetic correlations: for example, in an A(B) binary alloy with vacancies, the L_{BV} term of the Onsager matrix describes the correlations between the displacements of the solute atoms B and the vacancies V. If L_{BV} is positive, vacancy fluxes will drag solute atoms B so that solute will segregate in the vicinity of sinks, while if L_{BV} is negative, vacancy fluxes will induce solute flux in the opposite direction.

A cubic structure has an isotropic (scalar) Onsager matrix $L_{\alpha\beta}^0$, where α and β designate the different chemical species A, B, or V. The Onsager matrix is a non-linear function of the

atomic jump frequencies, and strain-induced symmetry breaking transforms each coefficient of the Onsager matrix into a strain-dependent second-rank tensor $\underline{L}^{ij}_{\alpha\beta}(\underline{\epsilon})$. For infinitesimal strains ϵ_{kl}, this dependency can be described using a fourth rank tensor $\underline{\underline{L'}} = \left(\frac{\partial L^{xy}_{\alpha\beta}}{\partial \varepsilon_{kl}}\right) = (L'^{xy,kl}_{\alpha\beta})$

$$\begin{aligned} L^{xy}_{\alpha\beta} &= L^{0}_{\alpha\beta}\delta_{(x,y)} + \sum_{\zeta,a,b,c} \frac{\partial L^{xy}_{\alpha\beta}}{\partial w^{(\zeta)}_{abc}} \frac{\partial w^{(\zeta)}_{abc}}{\partial \varepsilon_{kl}} \varepsilon_{kl} \\ &= L^{0}_{\alpha\beta} + \sum_{k,l} \frac{\partial L^{xy}_{\alpha\beta}}{\partial \varepsilon_{kl}} \varepsilon_{kl}, \end{aligned} \tag{3}$$

where δ is the Kronecker symbol. Considering a solid at mechanical equilibrium (no net torque), the strain tensor $\underline{\varepsilon}$ is a symmetric tensor. The fourth rank elasto-diffusion tensor $\underline{\underline{L'}}$ can be written more simply using the contracted Voigt notation of the elastic constants as it possesses identical symmetry. For a cubic structure $L'^{11}_{\alpha\beta} = L'^{22}_{\alpha\beta} = L'^{33}_{\alpha\beta}$, $L'^{12}_{\alpha\beta} = L'^{23}_{\alpha\beta} = L'^{13}_{\alpha\beta} = L'^{21}_{\alpha\beta} = L'^{32}_{\alpha\beta} = L'^{31}_{\alpha\beta}$ and $L'^{44}_{\alpha\beta} = L'^{55}_{\alpha\beta} = L'^{66}_{\alpha\beta}$. Thus, the knowledge of the Onsager matrix in the unstrained structure and of three of its derivatives is sufficient to describe the effect of any infinitesimal strain on the diffusion properties. However for larger strains, non-linearity can arise, in which case a specific calculation is necessary for each strain tensor. As a consequence, a comprehensive determination of strain effects on the Onsager matrix requires procedures sufficiently accurate to account for small perturbations and computationally efficient for multiple calculations in the non-linear case.

One approach to computing the Onsager matrix is to use analytic methods such as the self-consistent mean field (SCMF) method. This method allows quick and accurate computations of the Onsager matrix and has been used for several cubic structures[18,19], but no analytic calculation of the Onsager matrix of anisotropic structure has yet been presented. As the formalism introduced in Ref. 18 is able to tackle anisotropic structures, this method has been chosen to compute the Onsager matrix of two structures derived from the fcc structure by applying an elementary tetragonal strain ε_{33} and an elementary shear strain ε_{12}. From these two cases the whole elasto-diffusion tensor can be obtained in the linear limit using Eqn. 3. The SCMF solution finds a steady-state solution to the master equation on a lattice in the presence of an infinitesimal chemical potential gradient by considering thermodynamic averages of single and pair occupancies; in the dilute limit, all higher-order averages can be written in terms of single and pair averages, and so the expressions are exact.

In dilute alloys, a solute atom appreciably changes the energy landscape for a vacancy

out to a finite distance. Once this range is defined, the main approximation in SCMF calculations is the cut-off distance of the kinetic correlations. Beyond this range, the SCMF results converge exponentially with the number of "shells", where each additional shell is defined as the ensemble of sites that can be reached by one jump starting from any site of the previous shell[19]. DFT calculations of the Ni(Si) system found non-negligible solute-vacancy interactions up to a third nearest neighbor (NN) distance. As a consequence, SCMF calculations with four shells have been performed in this work, where the first shell includes 42 sites around the solute atom, corresponding to all the sites up to the third NN sites in the unstrained fcc structure. As the analytic expressions used in this work are cumbersome, they are not detailed here but are made available in the supplemental materials[31], as well as a Matlab® routine that directly computes the Onsager matrix from a set of atomic jump frequencies for each case presented.

Another approach to computing the Onsager matrix is using atomic kinetic Monte Carlo simulations[20,32,33]. This method does not involve any explicit spatial cut-off of the kinetic correlations[34]. As a consequence, it has been used in the current work to verify the analytic results in a few select cases. The Onsager Matrix is obtained using the Kubo-Green formula[35,36]:

$$L_{\alpha\beta} = \left\langle \frac{R_\alpha R_\beta}{6\Omega\tau} \right\rangle, \tag{4}$$

where Ω is the volume and R_α the total displacement of all atoms of type α during the integration time τ. We note here that the length of the Markov chains used in these simulations introduces a cut-off in term of the number of atomic jumps considered. This implies an increased computational cost of these simulations for highly-correlated systems involving very different frequencies. In such a case, the computation time required by this method limits in practice its accuracy and makes it unpractical for perturbative calculations.

As in Ref. 18 and 19, we chose in most cases to represent only the drag ratio $L_{\mathrm{BV}}/L_{\mathrm{BB}}$, where B designates the impurity. This quantity is sensitive to kinetic correlations as L_{BV} becomes positive when solute drag occurs, while L_{BB} is always positive and is used as a normalization constant. In the dilute limit, both L_{BV} and L_{BB} are proportional to the vacancy and the solute concentration. Hence, their ratio is independent from these concentrations. Similarly, their derivatives with respect to strain are also proportional to the vacancy and the solute concentration and are also represented normalized by L_{BB}. However, L_{AV}, L_{AA} and L_{VV} are proportional to the vacancy concentration but not the solute concentration. Thus,

for the sake of clarity, their derivatives with respect to strain are represented normalized by $\frac{L_{\mathrm{BB}}}{c_{\mathrm{B}}}$.

II. EFFECT OF STRAIN ON A MODEL FCC ALLOY WITH FIRST NN INTERACTIONS

Vacancy-mediated diffusion of impurities in a fcc structure can be described using the five-frequency model[37]. This model describes diffusion when solute-vacancy interactions only affect jumps involving the nearest-neighbor sites of the solute atoms. This simple model exhibits several possible kinetic behaviors, including solute drag by vacancies[19]. The effect of strain on diffusion is first studied by considering the effect of elementary strains on this model and their potential effect on the Onsager matrix.

A. Geometry and atomic jumps

Under an elementary strain ε_{33} our cubic crystal becomes face centered tetragonal with a ratio $c/a \neq 1$. The twelve first NN sites of the fcc structure are split into two symmetry classes: a group of four sites $\frac{a}{2}\langle 110\rangle$ written $1a$ and a group of eight sites $\frac{a}{2}\langle 011\rangle$ and $\frac{a}{2}\langle 101\rangle$ written $1b$. Thus, two different jump types are considered to model diffusion under a ε_{33} strain. Similarly, the solute-vacancy interactions are split into two groups. Hence, the five frequencies describing the migration of a vacancy in a dilute fcc alloy are split into fifteen different frequencies. These frequencies are conveniently designated using the nomenclature introduced in section I and are illustrated in Fig. 1. Three different frequencies, $w^{(1)}_{1a1b1b}, w^{(1)}_{1b1b1a}, w^{(1)}_{1b1a1b}$, describe the displacement of the vacancy around the solute; two jumps, $w^{(2)}_{1a}$ and $w^{(2)}_{1b}$, the solute-vacancy exchanges; four frequencies describe the dissociation of the solute-vacancy pair: $w^{(3)}_{1a\infty 1a}, w^{(3)}_{1a\infty 1b}$, $w^{(3)}_{1b\infty 1a}$ and $w^{(3)}_{1b\infty 1b}$ while four others describe their association: $w^{(4)}_{1a1a\infty}, w^{(4)}_{1a1b\infty}$, $w^{(4)}_{1b1a\infty}$ and $w^{(4)}_{1b1b\infty}$. Finally, two frequencies are now necessary to describe the displacement of the vacancy in the bulk: $w^{(0)}_{1a}$ and $w^{(0)}_{1b}$.

Similarly, a shear stress ε_{12} lower the cubic symmetry to a monoclinic structure with an angle $\gamma \neq \pi/2$, and splits the NN sites into three groups: a group $1a$ of two sites along the $\frac{a}{2}[\bar{1}10]$ direction, a group $1c$ of two sites along the $\frac{a}{2}[110]$ direction and a group $1b$ of the remaining eight sites $\frac{a}{2}\langle 101\rangle$ and $\frac{a}{2}\langle 011\rangle$. Then, the five frequencies of the fcc structures

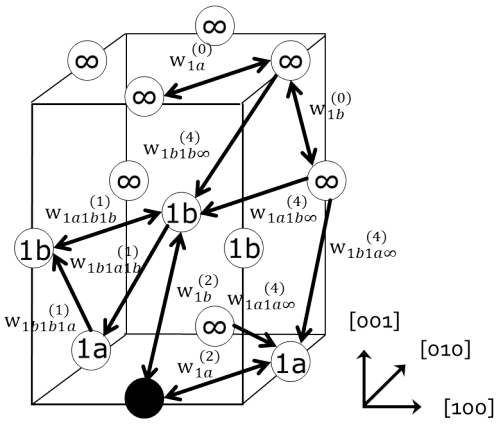

FIG. 1. Vacancy jump frequencies in a dilute FCC binary alloy with first NN interactions under a ε_{33} strain. Arrows indicate the direction of the vacancy jumps. The solute atom is represented by a filled circle, and on the other sites of the lattice, numbers describe the distance from the solute atom site with ∞ for sites beyond the range of the interactions. The $w^{(3)}_{i\infty j}$ corresponding to the return jumps of the $w^{(4)}_{ij\infty}$ jumps have been omitted for clarity.

are split into twenty eight frequencies: $w^{(0)}_{1a}, w^{(0)}_{1b}, w^{(0)}_{1c}, w^{(1)}_{1b\,1b\,1a}$, $w^{(1)}_{1b\,1a\,1b}, w^{(1)}_{1b\,1b\,1c}, w^{(1)}_{1b\,1c\,1b}, w^{(2)}_{1a}$, $w^{(2)}_{1b}, w^{(2)}_{1c}, w^{(3)}_{1a\,\infty\,1a}, w^{(3)}_{1a\,\infty\,1b}, w^{(3)}_{1a\,\infty\,1c}, w^{(3)}_{1b\,\infty\,1a}, w^{(3)}_{1b\,\infty\,1c}, w^{(3)}_{1c\,\infty\,1a}, w^{(3)}_{1c\,\infty\,1b}, w^{(3)}_{1c\,\infty\,1c}, w^{(4)}_{1b\,1b\,\infty}, w^{(4)}_{1a\,1b\,\infty}, w^{(4)}_{1a\,1c\,\infty}$, $w^{(4)}_{1b\,1a\,\infty}, w^{(4)}_{1b\,1b\,\infty}, w^{(4)}_{1b\,1c\,\infty}$, $w^{(4)}_{1c\,1a\,\infty}, w^{(4)}_{1c\,1b\,\infty}$ and $w^{(4)}_{1c\,1c\,\infty}$. Fig. 2 shows the specific exchanges corresponding to these frequencies. Note that all $1a$ jumps are parallel, as well as $1c$ jumps.

B. Solute drag in a model alloy under tetragonal strain

We consider here the case of a fcc lattice under an elementary strain ε_{33}. In an approach similar to the one used in Ref. 18, the effect of each frequency on the drag ratio of an model system with no heat of solution has first been studied. Due to detailed balance, all the frequencies corresponding to solute-vacancy pair dissociation are equal to the corresponding association frequencies. Similarly, for jumps of the vacancy around the solute, the equality $w^{(1)}_{1b\,1b\,1a} = w^{(1)}_{1b\,1a\,1b}$ holds. The results of SCMF calculations for the different remaining independent frequencies are shown on Fig. 3 with the drag ratio both in the [001] and in the [010] directions.

The frequencies $w^{(2)}_{1a}$ and $w^{(2)}_{1b}$ have no effect on the drag ratio, and the effect of each of the association or rotation frequencies are presented on Fig. 3 both along the [001] direction

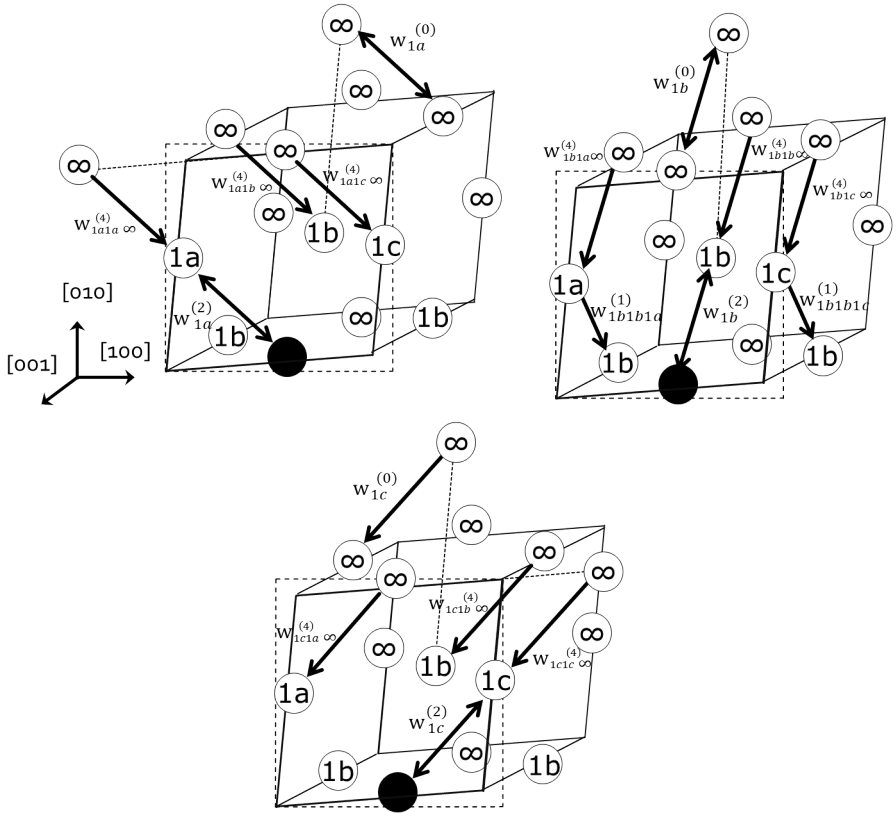

FIG. 2. Vacancy jump frequencies in a dilute FCC binary alloy with first NN interactions under a ε_{12} strain. Arrows indicate the direction of the vacancy jumps. The solute atom is represented by a filled circle, and on the other sites of the lattice, numbers describe the distance from the solute atom site with an ∞ signs for the sites beyond the range of the interactions. The $w^{(3)}_{i\infty j}$ corresponding to the return jumps of the $w^{(4)}_{ij\infty}$ jumps have been omitted for clarity.

and the [010] direction. First, the symmetry breaking at the atomic scale due to strain is reflected at the mesoscopic scale, as the drag ratio in the [001] direction differs from the drag ratio in the [010] direction. We observe that some of the different frequencies of the strained structure taken independently can cause solute drag when they are much larger than the jump frequency in the bulk. In comparison, both small and large values of the association/dissociation frequency $w^{(4)}_{11\infty}$ of the unstrained fcc structure can cause solute drag. In this last case, solute drag is due to a trapping effect; such trapping occurs in the strained case by a combination of lowering and raising the strain-split association and dissociation frequencies.

To further investigate the potential effect of strain-induced splitting, we scale all of these

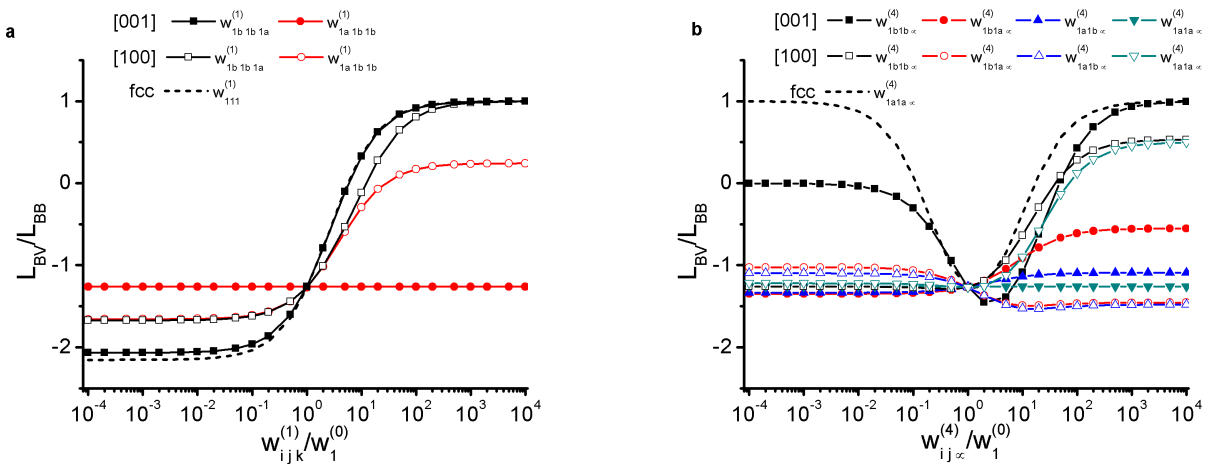

FIG. 3. (color online) Drag ratio $L_{\rm BV}/L_{\rm BB}$ of a model alloy under an elementary strain ε_{33} as a function of (a) the different frequencies corresponding to $w^{(1)}_{111}$ in the fcc structure, (b) the different frequencies corresponding to $w^{(4)}_{11\infty}$ in the fcc structure. Filled symbols correspond to fluxes along the [001] direction, empty symbols to fluxes along the [100] or [010] direction. The corresponding ratio in the fcc structure is indicated by a dashed line.

jumps along the $1b$ direction by a common factor φ and compute the drag ratio. As the $w^{(1)}_{111}$ frequency of the fcc structure plays an important role in the onset of solute drag by controlling the 1-orbit[19], the effect of a simultaneous variation by a factor ψ of all the split frequencies originating from $w^{(1)}_{111}$ has been also studied. Fig. 4 shows contour plots for variations of these two parameters φ and ψ. A large splitting coefficient φ reduces solute drag in the [001] direction, while leaving the limit of solute drag in the (001) plane unchanged. Thus, from both the single frequency parametric study and the (φ, ψ) study, strain-induced frequency splitting appears to be likely to reduce solute drag.

C. Solute drag in a model alloy under shear strain

An elementary shear strain ε_{12} splits the five frequencies of the fcc lattice into 28 different frequencies, which can be organized in three groups according to the jump distance. These groups are illustrated on Fig. 2. However, the potential effect of shear strain can be understood with a splitting parameter χ such that for all ζ, i, j, $w^{(\zeta)}_{1aij} = \chi, w^{(\zeta)}_{1bij} = 1$ and $w^{(\zeta)}_{1cij} = \chi^{-1}$. This model describes the effect of a linear variation with ϵ_{12} of all the migration barrier by a same amount. Drag ratios for different values of χ have been obtained

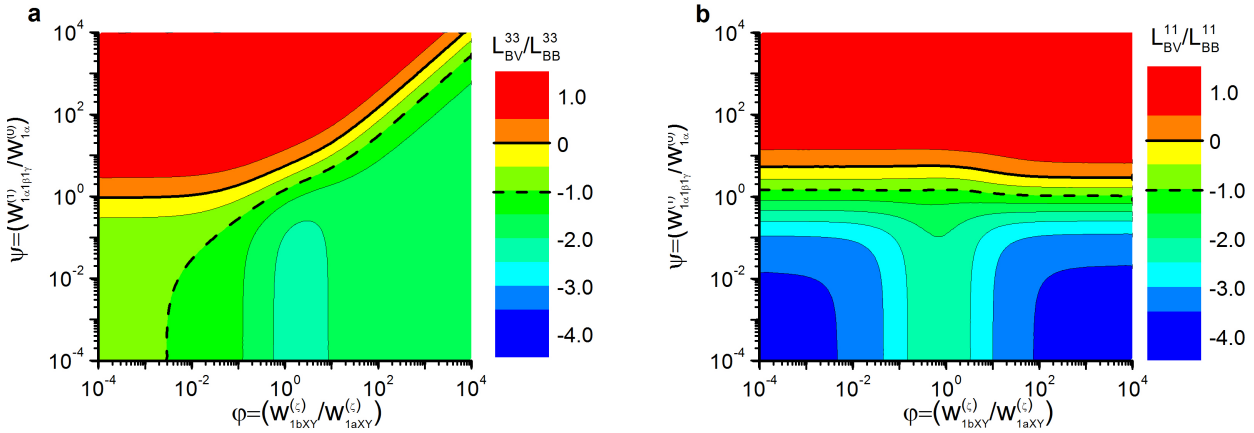

FIG. 4. (color online) Contour map of the drag ratio $L_{\mathrm{BV}}/L_{\mathrm{BB}}$ of a model alloy under an elementary strain ε_{33} in (a) the [001] direction and (b) the [100] direction as a function of the splitting parameter φ and the 1-orbit parameter ψ (for all i,j,k, $w_{ijk}^{(1)}/w_i^{(0)}=\psi$, and for all j,k,ζ, $w_{1bjk}^{(\zeta)}/w_{1ajk}^{(\zeta)}=\varphi$). The solid line indicates the onset of solute drag, while the dashed line for $L_{\mathrm{BV}}=-L_{\mathrm{BB}}$ is a guide to the eye.

using SCMF calculations and compared with AKMC simulations. In these simulations, a simple-cubic supercell of the fcc cell containing $4\times6\times6\times6$ sites, including one occupied by a B atom and one by a vacancy, is first equilibrated for 100 Monte Carlo steps (where each step corresponds to $4\times6\times6\times6$ transitions). Then kinetic correlations are computed over 100 Monte Carlo steps, and averaged over 10^6 trajectories.

Fig. 5 shows the drag ratios in the [001] and the (001) plane. A very good agreement is obtained between AKMC simulations and SCMF calculation for values of χ covering two decades in the [001] direction, but in the (001) plane the agreement becomes poorer for $\chi>20$. Moreover, in that direction, the drag ratio drops abruptly for very large values of χ. This behavior can be understood by observing that in that case, diffusion occurs primarily only along parallel lines (cf. Fig. 2). Thus, we expect a behavior similar to a one-dimensional chain, where the L_{BB} term vanishes as the chain length increases[38–40]. Indeed, in the case of $\chi\gg1$, $L_{\mathrm{BB}}\to0$, which induces the divergence of the drag ratio. The slight discrepancy observed for $\chi>20$ is due to a too small integration time of the AKMC simulations, as well as to the truncation of kinetic correlations in SCMF calculations.

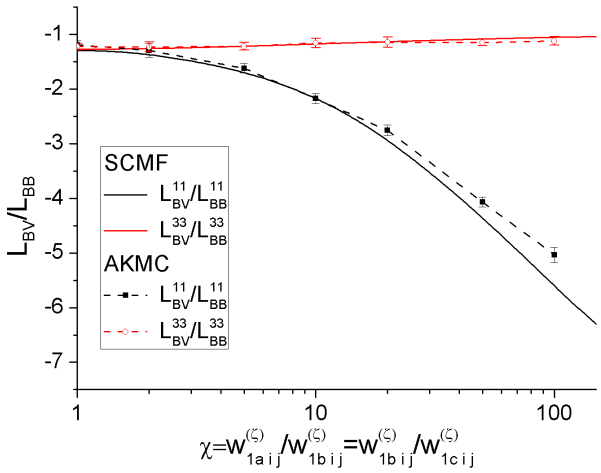

FIG. 5. Drag ratio $L_{\rm BV}/L_{\rm BB}$ in the [001] direction and in the (001) plane of a model alloy under an elementary strain ε_{12} as a function of χ (for allζ, i, j, $w^{(\zeta)}_{1a\,ij} = \chi, w^{(\zeta)}_{1b\,ij} = 1$ and $w^{(\zeta)}_{1c\,ij} = \chi^{-1}$). Symbols indicate results of AKMC simulations, with error bars computed from their statistical standard deviation, and the solid line is the SCMF result.

III. DIFFUSION OF SI IMPURITIES IN NI UNDER STRAIN

Previously, atomic-scale migration properties of Si impurities in Ni were computed using DFT[28]. In this fcc alloy, non-negligible solute-vacancy interactions are found up to the third NN sites thus requiring the calculation of sixteen frequencies to describe diffusion. Moreover, the effect of infinitesimal strains on each of the sixteen migration barrier has been computed, providing all the information required to study strain effects on diffusion in this alloy. This work showed that migration barriers depends linearly on strain up to $\varepsilon = 0.01$.

Under a tetragonal strain ε_{33}, the first, second and third NN distances of a fcc structure are split into six different distances, and the sixteen frequencies are split into forty-four different frequencies. These forty-four frequencies are represented on Fig. 6 and listed in the App. A. The values of these forty-four frequencies can be deduced from the migration barriers $E^{\rm mig}_i$ of the 16 jumps of the unstrained case and the elastic dipole $\underline{P}$ of each jump using relationships of the type $E^{\rm mig}_j(\varepsilon) = E^{\rm mig}_i + \sum_{p,q,k,l} \Theta_j(P_{pq})\varepsilon_{kl}$, where Θ_j is a rotation operator. In the present case, using data from Ref. 28, the migration barrier is $E^{m,\zeta}_{1a\,i\,j}(\varepsilon) = E^{m,\zeta}_{1ij} + (8.09\text{ eV})\varepsilon_{33}$ for a jump in the $1a$ direction, and $E^{m,\zeta}_{1bij}(\varepsilon) = E^{m,\zeta}_{1ij} - (14.88\text{ eV})\varepsilon_{33}$ in the $1b$ direction. A similar approach can be used to describe the effect of a shear strain

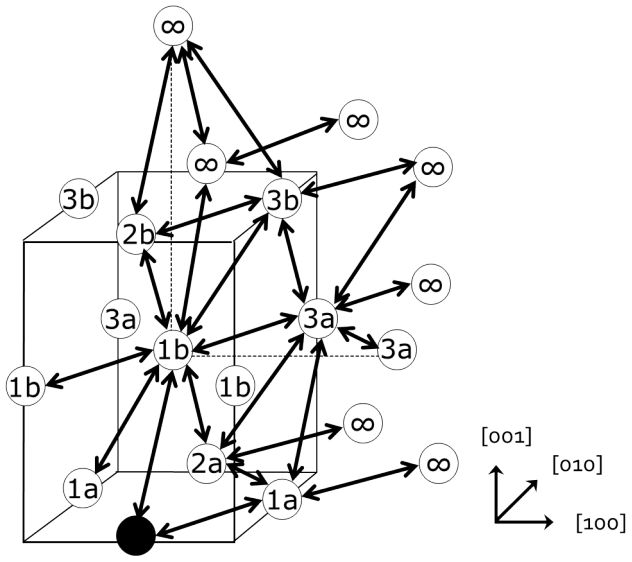

FIG. 6. Vacancy jump frequencies in a dilute FCC binary alloy with first, second and third NN interactions under a ε_{33} strain. Arrows indicate the direction of the vacancy jumps. The solute atom is represented by a filled circle, and on the other sites of the lattice the numbers describe the distance from the solute atom site with an ∞ sign for the sites beyond the range of the interactions.

ε_{12}. In that case, nine different types of sites are within interaction range of the solute, and the sixteen frequencies are split into eighty-four frequencies. SCMF calculations have been performed for both tetragonal ($\varepsilon_{33} \neq 0$) and monoclinic ($\varepsilon_{12} \neq 0$)cases to determine the elasto-diffusion tensor. Effects of strain beyond the linear regime were also investigated using SCMF calculations in the tetragonal case.

A. Linear regime

Using data from Ref. 28, the Onsager matrix in the absence of strain has first been computed using the SCMF method. The diagonal terms for the two atomic species are represented in a logarithmic plot in Fig. 7 for a calculation with a solute concentration $c_{\mathrm{Si}} = 10^{-4}$. While the impurity coefficients display approximately Arrhenian behavior, the Ni term is non-Arrhenian beyond room temperature. For the linear limit in c_{Si}, $L_{\mathrm{NiNi}} = \frac{1}{2a} c_v w_1^{(0)} (1 + c_{\mathrm{Si}} b)$ where a is the lattice parameter and b is the "solute enhancement factor,"[17] which is a function of the sixteen different frequencies. At high temperatures L_{NiNi} is dominated by $w_1^{(0)}$, as expected. Considering the solute-vacancy complex at distance z with binding

energy E_z^b, if it has jumps such that $E_{xyz}^{\mathrm{mig},\zeta} + E_z^b < E_1^{\mathrm{mig},0}$, the solute enhancement term dominates at low temperature, unless the solute concentration is strictly null. This is the case for the Ni(Si) alloy as shown in Fig. 7, where the two asymptotic regimes associated with frequencies $w_1^{(0)}$ and $w_{111}^{(1)}$ are represented as obtained from the bare mobility[1941]. The crossover between the two regimes depends strongly on the difference of migration barriers and to a lesser extent on the solute concentration. As the non-diagonal term L_{BV} changes sign at $T \approx 1060K$, this term does not follow an Arrhenius relation either and cannot be represented on a logarithmic plot. Thus, it is represented normalized by L_{SiSi} in Fig. 8.

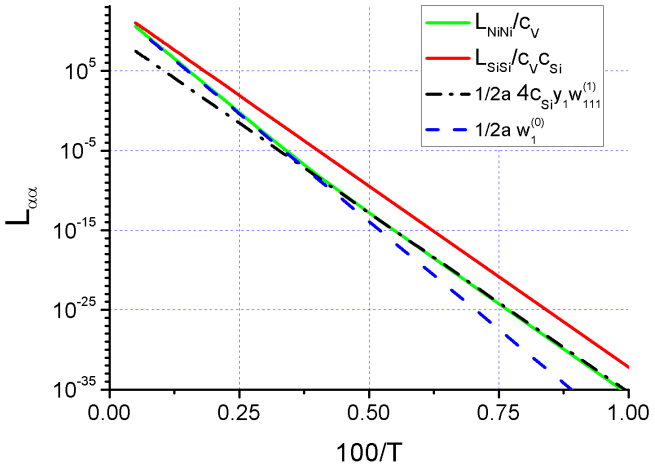

FIG. 7. (color online) Diagonal terms of the Onsager matrix as a function of the temperature for the Ni(Si) alloy. The Ni term is green and the impurity term is red. The two asymptotic regimes associated to the frequencies $w_1^{(0)}$ and $w_{111}^{(1)}$ are represented as extracted from the bare mobility[19], where $y_1 = exp(-E_1^b/(k_{\mathrm{B}}T))$ is the exponential of the first NN binding energy.

We compute the elasto-diffusion tensor using the SCMF method. In the Ni(Si) alloy, the cross terms of the elastic dipole—which quantifies the effect of ε_{12} shear strain on diffusion—are all an order of magnitude smaller than the diagonal terms[28]. It was assumed in Ref. 27 that the effects of a shear strain on diffusion could be neglected for this alloy. This assumption has been assessed by computing the $L_{\alpha\beta}^{\prime 66}$ terms of the elasto-diffusion tensor, which describes the effect of shear strain. A value $L_{\alpha\beta}^{\prime 66}/L_{\alpha\beta} = 1 \pm 0.02$ was found for all temperature and chemical species, expressing the fact that shear strain affects diffusion only through the geometrical deformation of the lattice and that its effect on the diffusion barrier is negligible. Fig. 9 shows values of the other derivatives. At low temperature, these deriva-

tives are inversely proportional to the temperature, in agreement with an Arrhenian relation for the Onsager matrix and a linear dependency of the activation energy with strain, with $L'^{11}_{SiSi} = L'^{11}_{SiV}$ and $L'^{12}_{SiSi} = L'^{12}_{SiV}$ as in the low temperature limit $L_{\mathrm{SiV}} = L_{\mathrm{SiSi}}$. Beyond room temperature, this linear behavior disappears at a temperature similar to the one observed for the terms of the Onsager matrix. Moreover L'^{12}_{SiV} and L'^{11}_{SiV} change sign and become negative.

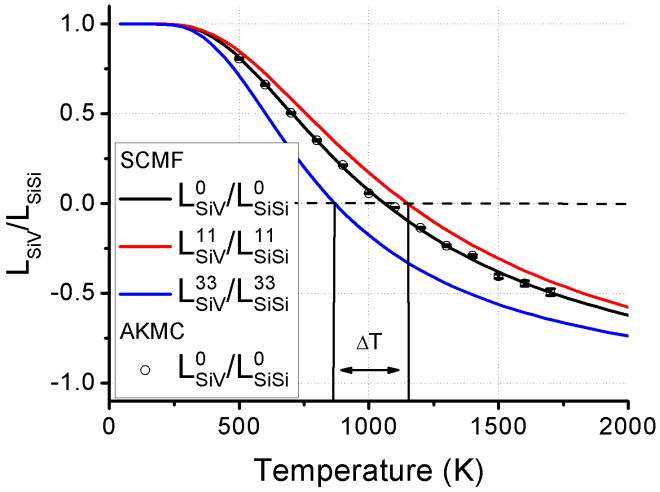

FIG. 8. (color online) $L_{\mathrm{BV}}/L_{\mathrm{BB}}$ ratio for the Ni(Si) alloy in the absence of strain (solid line for SCMF results, circles for AKMC results) and under a tetragonal tensile strain $\varepsilon_{33} = -2\varepsilon_{11} = -2\varepsilon_{22} = \varepsilon = 0.01$ as a function of the temperature in the [100] direction (dashed line) and in the [010] direction (dotted line). The error bars represent the statistical variance of AKMC simulations.

B. Effect of finite strains on Si diffusion

In order to study the effect of a finite strain on diffusion properties, a constant-volume tetragonal strain has been applied to the fcc structure: $\varepsilon = \varepsilon_{33} = -2\varepsilon_{11} = -2\varepsilon_{22}$ and $\varepsilon_{13} = \varepsilon_{12} = \varepsilon_{23} = 0$. In this case the structure becomes tetragonal as in the case of the simple ε_{33} strain. Fig. 8 shows the effect of this strain tensor on drag ratios. In the unstrained case, solute drag occurs at low temperature and disappears at a temperature $T_c \approx 1060K$. This behavior is expected for fcc alloys with attractive solute-vacancy interactions[19], with T_c scaling approximately with the strength of this interaction. The symmetry breaking induced at the atomic scale by the strain tensor is reflected in the mesoscale transport

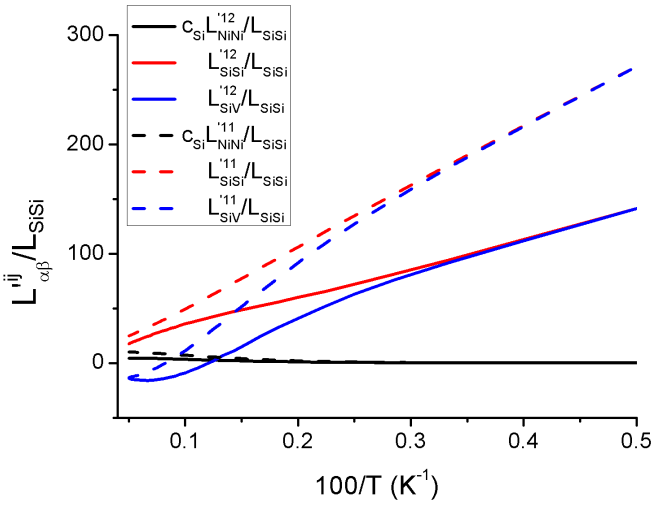

FIG. 9. (color online) Derivatives of the Onsager matrix of the Ni(Si) alloy with respect to strain. The L'^{11} are dashed lines and the L'^{12} terms are solid, with black for the matrix term, red for the impurity term and blue for the vacancy-impurity correlation.

coefficients. Moreover, Fig. 8 shows that strain can change even the nature of solute drag: for a strain-dependent range of temperatures $\Delta T(\varepsilon)$ around the transition temperature T_c, the drag ratio is negative in the [100] direction and positive in its normal plane. Thus, in this range of temperature, solute atoms follow the vacancies in the (100) plane, but diffuse in the opposite direction in the [100] direction, which can lead to non-trivial diffusion patterns around defects that generate stress fields[27].

In order to verify the accuracy of these calculations, the Onsager matrix of the Ni(Si) alloy was been computed using SCMF calculations and AKMC simulations. AKMC simulations were performed using a $4 \times 6 \times 6 \times 6$ site supercell as before, integrating trajectories over 10 Monte Carlo and averaging the results over 10^5 trajectories. An excellent agreement is achieved at all temperatures between AKMC and SCMF results.

The Onsager matrix is a highly non-linear function of the jump frequencies. Thus, the linearity of the migration barriers with respect to strain does not ensure the linearity of the Onsager matrix with respect to strain. This non-linearity is striking in the case of the Ni(Si) system under tetragonal compression $\varepsilon_{33} = -2\varepsilon_{11} = -2\varepsilon_{22} = \varepsilon < 0$. In the linear limit, $L^{33}_{\alpha\beta} = -2L^{11}_{\alpha\beta} = -2L^{22}_{\alpha\beta}$. However, non-linear effects arise at low strain, as shown on Fig. 10. For $\varepsilon < -0.005$, the drag ratio suddenly drops at low temperatures, leading to the complete elimination of solute drag. This phenomenon can be understood by observing the effect of

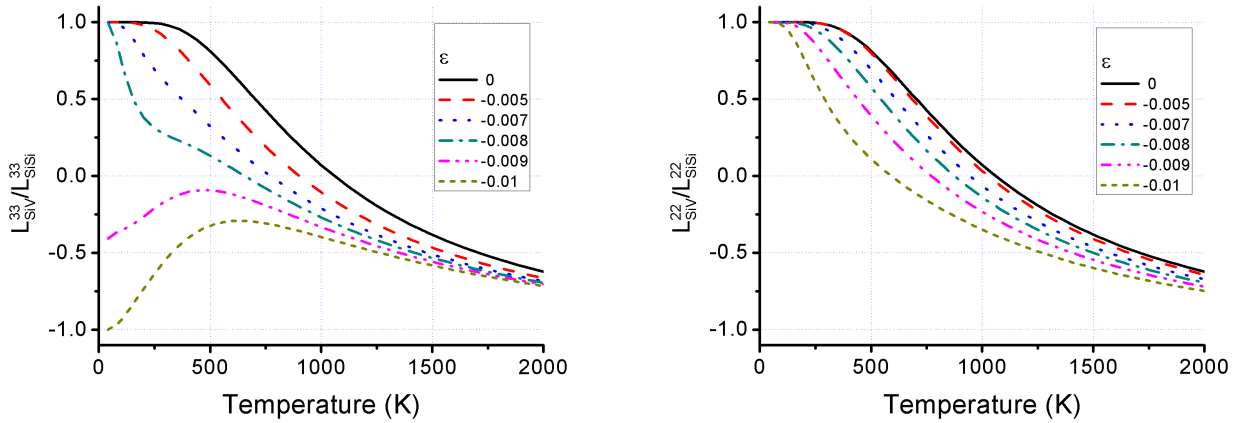

FIG. 10. (color online) $L_{\mathrm{BV}}/L_{\mathrm{BB}}$ ratio for the Ni(Si) alloy under a tetragonal compressive strain $\varepsilon_{33} = -2\varepsilon_{11} = -2\varepsilon_{22} = \varepsilon < 0$ as a function of the temperature and ε along the [100] direction (left) and the [010] directions (right).

strain on each frequency. As shown in Ref. 28, the main effect of this strain is to increase the migration barrier along the strain axis, and to decrease the migration barrier in the normal plane. This decrease facilitates the escape of the vacancy from the neighborhood of the solute without contributing to solute drag along the strain axis: $w^{(1)}_{1b1a1b}$ is responsible for solute drag in the [001] direction, and while at low temperature for $\varepsilon = -0.008$, $w^{(1)}_{1a2a1a} < w^{(1)}_{1b1a1b}$, for $\varepsilon = -0.009$, $w^{(1)}_{1a2a1a} > w^{(1)}_{1b1a1b}$; the vacancy can then move from the first to the second NN sites and from there escape to the bulk. Hence, this splitting of the frequencies contributes to the reduction of solute drag along the strain axis. Similarly, while this strain tensor increases the drag ratio for small $|\varepsilon|$, nonlinear effects induce its decrease for $-\varepsilon > 0.002$. Thus, a compressive tetragonal strain can suppress solute drag in *all* directions.

IV. CONCLUSION

The sensitivity of solute drag to stress depends on the strength of solute drag in the underlying material system, and furthermore on the underlying crystal structure. For example, we expect that closed-packed structures, like FCC and HCP, would have stronger solute-drag stress-sensitivity than more open structures, like BCC. A first result of this work is to provide analytic expressions of the Onsager matrix obtained using the SCMF method in the case of a FCC structure. They are now available for quick and accurate calculation

of vacancy-mediated diffusion in crystal structures derived from the fcc structure, for vacancy solute interactions up to the third NN sites. They have been assessed on select cases using AKMC simulations, illustrating the ability of SCMF calculations to treat anisotropic systems.

These expressions have been used to evaluate the effect of strain on diffusion in fcc structures. The splitting of the atomic jump frequencies by strain leads to a symmetry breaking of the Onsager matrix. A rich anisotropic behavior of the Onsager matrix has been observed for the model case of an alloy with no heat of mixing on an fcc structure with first NN solute-vacancy interactions under strain, where in most studied cases strain reduces solute drag.

The effect of a tetragonal strain on the Onsager matrix of the Ni(Si) alloy has been studied. The elasto-diffusion tensor has been computed, providing access to the whole linear regime. We show that the different components of the elasto-diffusion tensors have a non-Arrhenian behavior and can change sign at a temperature equivalent to the temperature T_c at which solute drag disappears. Furthermore, the effects of a volume-conserving tetragonal strain have been computed beyond the linear regime. It shows that a tensile strain can create a temperature range in which qualitatively different behaviors take place along the strain axis and perpendicular. Under a compressive strain, the strong non-linear behavior induces a reduction of solute drag in all directions. It should be underlined that, as illustrated in the case of the Ni(Si) alloy, the linearity of the effect of strain on the migration barrier does not imply a linear behavior of diffusion properties. Thus, in applications where solute drag would appear to be a hindrance, the non-linear behavior of the Onsager matrix could be used to suppress solute drag by applying a controlled strain to the material.

V. ACKNOWLEDGEMENTS

The authors thank J. L. Bocquet for his continuous interest for this work and his remarks. This research is partly supported by the DOE-BES grant DE-FG02-05ER46217, and by the DOE-BES Computation Materials and Chemical Sciences Network on "Computational Microstructure Science".

Appendix A: Frequencies involved in the case of a fcc structure with third NN interactions under a ε_{33} strain

List of the 44 frequencies involved in diffusion in a fcc structure under a ε_{33} strain: $w^{(0)}_{1a}$, $w^{(0)}_{1b}$, $w^{(1)}_{1a\,1a\,2a}$, $w^{(1)}_{1a\,1a\,1b}$, $w^{(1)}_{1a\,2a\,1a}$, $w^{(1)}_{1b\,1a\,1b}$, $w^{(1)}_{1b\,1b\,1a}$, $w^{(1)}_{1b\,1b\,2a}$, $w^{(1)}_{1b\,2a\,1b}$, $w^{(1)}_{1b\,3b\,1b}$, $w^{(1)}_{1a\,2b\,3b}$, $w^{(1)}_{1a\,3a\,3a}$, $w^{(1)}_{1a\,3b\,2b}$, $w^{(1)}_{1b\,3a\,3b}$, $w^{(1)}_{1b\,3b\,3a}$, $w^{(1)}_{1a\,1b\,3a}$, $w^{(1)}_{1a\,3a\,1b}$, $w^{(1)}_{1b\,1a\,3a}$, $w^{(1)}_{1b\,1b\,2b}$, $w^{(1)}_{1b\,2b\,1b}$, $w^{(1)}_{1b\,3a\,1a}$, $w^{(1)}_{1b\,1b\,3b}$, $w^{(1)}_{1b\,2a\,3a}$, $w^{(1)}_{1b\,3a\,2a}$, $w^{(2)}_{1a}$, $w^{(2)}_{1b}$, $w^{(3)}_{1a\,\infty\,1a}$, $w^{(3)}_{1a\,\infty\,2a}$, $w^{(3)}_{1b\,\infty\,1b}$, $w^{(3)}_{1b\,\infty\,2a}$, $w^{(3)}_{1a\,\infty\,3a}$, $w^{(3)}_{1b\,\infty\,2b}$, $w^{(3)}_{1a\,\infty 3b}$, $w^{(3)}_{1b\,\infty 3a}$, $w^{(3)}_{1b\,\infty 3b}$, $w^{(4)}_{1a\,1\infty}$, $w^{(4)}_{1a\,2a\infty}$, $w^{(4)}_{1b\,1b\infty}$, $w^{(4)}_{1b\,2a\infty}$, $w^{(4)}_{1a\,3a\,\infty}$, $w^{(4)}_{1b\,2b\infty}$, $w^{(4)}_{1a\,3b\,\infty}$, $w^{(4)}_{1b\,3a\,\infty}$, $w^{(4)}_{1b\,3b\,\infty}$.

Appendix B: Frequencies involved in the case of a fcc structure with third NN interactions under a ε_{12} strain

List of the 84 frequencies involved in diffusion in a fcc structure under a ε_{12} strain: $w^{(0)}_{1a}$, $w^{(0)}_{1b}$, $w^{(0)}_{1c}$, $w^{(2)}_{1a}$, $w^{(2)}_{1b}$, $w^{(2)}_{1c}$, $w^{(1)}_{1a\,1b\,1b}$, $w^{(1)}_{1a\,1b\,3a}$, $w^{(1)}_{1a\,1c\,2b}$, $w^{(1)}_{1a\,2a\,2c}$, $w^{(1)}_{1a\,2b\,1c}$, $w^{(1)}_{1a\,2c\,2a}$, $w^{(1)}_{1a\,3a\,1b}$, $w^{(1)}_{1a\,3c\,3c}$, $w^{(1)}_{1b\,1a\,1b}$, $w^{(1)}_{1b\,1a\,3a}$, $w^{(1)}_{1b\,1b\,1a}$, $w^{(1)}_{1b\,1b\,1c}$, $w^{(1)}_{1b\,1b\,2a}$, $w^{(1)}_{1b\,1b\,2b}$, $w^{(1)}_{1b\,1b\,2c}$, $w^{(1)}_{1b\,1b\,3b}$, $w^{(1)}_{1b\,1c\,1b}$, $w^{(1)}_{1b\,1c\,3c}$, $w^{(1)}_{1b\,2a\,1b}$, $w^{(1)}_{1b\,2b\,1b}$, $w^{(1)}_{1b\,2b\,3a}$, $w^{(1)}_{1b\,2b\,3c}$, $w^{(1)}_{1b\,2c\,1b}$, $w^{(1)}_{1b\,2c\,3a}$, $w^{(1)}_{1b\,3a\,1a}$, $w^{(1)}_{1b\,3a\,2b}$, $w^{(1)}_{1b\,3a\,2c}$, $w^{(1)}_{1b\,3b\,1b}$, $w^{(1)}_{1b\,3b\,3c}$, $w^{(1)}_{1b\,3c\,1c}$, $w^{(1)}_{1b\,3c\,2b}$, $w^{(1)}_{1b\,3c\,3b}$, $w^{(1)}_{1c\,1a\,2b}$, $w^{(1)}_{1c\,1b\,1b}$, $w^{(1)}_{1c\,1b\,3c}$, $w^{(1)}_{1c\,2a\,3b}$, $w^{(1)}_{1c\,2b\,1a}$, $w^{(1)}_{1c\,3a\,3a}$, $w^{(1)}_{1c\,3b\,2a}$, $w^{(1)}_{1c\,3c\,1b}$, $w^{(3)}_{1a\,\infty\,1a}$, $w^{(3)}_{1a\,\infty\,2b}$, $w^{(3)}_{1a\,\infty\,2c}$, $w^{(3)}_{1a\,\infty\,3a}$, $w^{(3)}_{1a\,\infty\,3b}$, $w^{(3)}_{1a\,\infty\,3c}$, $w^{(3)}_{1b\,\infty\,1b}$, $w^{(3)}_{1b\,\infty\,2a}$, $w^{(3)}_{1b\,\infty\,2b}$, $w^{(3)}_{1b\,\infty\,2c}$, $w^{(3)}_{1b\,\infty\,3a}$, $w^{(3)}_{1b\,\infty\,3b}$, $w^{(3)}_{1b\,\infty\,3c}$, $w^{(3)}_{1c\,\infty\,1c}$, $w^{(3)}_{1c\,\infty\,2b}$, $w^{(3)}_{1c\,\infty\,2c}$, $w^{(3)}_{1c\,\infty\,3a}$, $w^{(3)}_{1c\,\infty\,3b}$, $w^{(3)}_{1c\,\infty\,3c}$, $w^{(4)}_{1a\,1a\,\infty}$, $w^{(4)}_{1a\,2b\,\infty}$, $w^{(4)}_{1a\,2c\,\infty}$, $w^{(4)}_{1a\,3a\,\infty}$, $w^{(4)}_{1a\,3b\,\infty}$, $w^{(4)}_{1a\,3c\,\infty}$, $w^{(4)}_{1b\,1b\,\infty}$, $w^{(4)}_{1b\,2a\,\infty}$, $w^{(4)}_{1b\,2b\,\infty}$, $w^{(4)}_{1b\,2c\,\infty}$, $w^{(4)}_{1b\,3a\,\infty}$, $w^{(4)}_{1b\,3b\,\infty}$, $w^{(4)}_{1b\,3c\,\infty}$, $w^{(4)}_{1c\,1c\,\infty}$, $w^{(4)}_{1c\,2b\,\infty}$, $w^{(4)}_{1c\,2c\,\infty}$, $w^{(4)}_{1c\,3a\,\infty}$, $w^{(4)}_{1c\,3b\,\infty}$, $w^{(4)}_{1c\,3c\,\infty}$.

---

* tgarnier@illinois.edu

[1] V. I. Yelagin, V. V. Zakharov, S. G. Pavlenko, and T. D. Rostova, Phys. Met. Metall. **60**, 88–92 (1986).

[2] E. Clouet, L. Laé, T. Épicier, W. Lefebvre, M. Nastar, and A. Deschamps, Nat. Mater. **5**, 482 (2006).

[3] F. Danoix, E. Bemont, P. Maugis, and D. Blavette, Adv Eng. Mat. **8**, 1202 (2006).

[4] Z. Mao, C. K. Sudbrack, K. E. Yoon, G. Martin, and D. N. Seidman, Nature Materials **6**, 210 (2007).

[5] G. Martin, Phys. Rev. B **30**, 1424 (1984).

[6] A. Barbu and G. Martin, Scripta Metallurgica, **11**, 771 (1977).

[7] A. Barbu, G. Martin, and A. Chamberod, J. Appl. Phys **51**, 6182 (1980).

[8] M. Nastar and F. Soisson, "Comprehensive nuclear materials," (Elsevier, 2012) Chap. Radiation induced segregation, pp. 471–496.

[9] Z. Jiao and G. Was, Acta Materialia **59**, 1220 (2011).

[10] P. H. Dederichs and K. Schroeder, Phys. Rev. B **17**, 2524 (1978).

[11] Savino, Phil. Mag. **36**, 323 (1978).

[12] V. Vaithyanathan, C. Wolverton, and L. Q. Chen, Phys. Rev. Lett. **88**, 125503 (2002).

[13] W. Chan, A. R.S., and Y. Ashkenazy, J. Appl. Phys **104**, 023502 (2008).

[14] J. Bocquet, Acta Metall. **22**, 1 (1974).

[15] Y. Okamura and A. R. Allnatt, Journal of Physics C: Solid State Physics **16**, 1841 (1983).

[16] G. E. Murch and S. Rothman, JOM **35**, A42 (1983).

[17] M. Nastar, Philosophical Magazine **85**, 3767 (2005).

[18] T. Garnier, M. Nastar, P. Bellon, and D. R. Trinkle, Phys. Rev. B **88**, 134201 (2013).

[19] T. Garnier, D. R. Trinkle, M. Nastar, and P. Bellon, Phys. Rev. B **89**, 144202 (2014).

[20] A. Van der Ven and G. Ceder, Phys. Rev. Lett. **94**, 045901 (2005).

[21] A. V. Barashev and A. C. Arokiam, Philos. Mag. Lett. Vol. **86**, 321 (2006).

[22] F. Soisson and C. C. Fu, Phys. Rev. B **76**, 214102 (2007).

[23] P. Ghate, Phys. Rev. **133 (4A)**, 1167 (1964).

[24] M. Koiwa and S. Ishioka, Phil. Mag.A **47(5)**, 767 (1983).

[25] A. Van der Ven, G. Ceder, M. Asta, and P. D. Tepesch, Phys. Rev. B **64**, 184307 (2001).

[26] S. Ganeshan, L. Hector Jr, and Z. Liu, Acta Materialia **59**, 3214 (2011).

[27] T. Garnier, V. R. Manga, D. R. Trinkle, M. Nastar, and P. Bellon, Phys. Rev. B **88**, 134108 (2013).

[28] T. Garnier, V. R. Manga, D. Trinkle, and P. Bellon, Phys. Rev. B in press.

[29] G. Vineyard, Journal of Physics and Chemistry of Solids, **3**, 121 (1957).

[30] N. Pottier, *Physique statistique hors d'équilibre : Processus irréversibles linéaires* (EDP-sciences, 2007).

[31] For the supplemental materials, see http://link.aps.org/supplemental/XXXXXXX . A routine computing the Onsager matrix for a fcc structure under tetragonal strain from a set of fourty-

four frequency is provided, as well as a similar routine for the sheared fcc structure.

[32] A. R. Allnatt and A. B. Lidiard, *Atomic Transport in Solids* (Cambridge University Press, 1993).

[33] T. Garnier and M. Nastar, Phys. Rev. B **88**, 134207 (2013).

[34] The finite length of the Markov chains used in practice in these simulations acts as an implicit cut-off of the kinetic correlation in Monte Carlo simulations.

[35] A. R. Allnatt, Journal of Physics C: Solid State Physics **15**, 5605 (1982).

[36] A. R. Allnatt and E. L. Allnatt, Phil. Mag. A **49(5)**, 625 (1984).

[37] R. Howard and A. Lidiard, J. Phys. Soc. Jap. Suppl II **18**, 197 (1963).

[38] A. Hodgkin and R. Keynes, J. phys. **128**, 61 (1955).

[39] E. J. Harris, *Transport and Accumulation in Biological Systems*, edited by London (Butterworths Scientific Publications, 1960).

[40] H. van Beijeren, K. W. Kehr, and R. Kutner, Phys. Rev. B **28**, 5711 (1983).

[41] As in the case of the Ni(Si) alloy the solute-vacancy exchange has an even lower migration barrier, the correlation term of the Onsager matrix becomes negligible at low temperature compared to the bare mobility of Ni atom.